Chemical Science

ROYAL SOCIETY OF CHEMISTRY

EDGE ARTICLE

View Article Online
View Journal | View Issue

Cite this: *Chem. Sci.*, 2026, **17**, 1002

All publication charges for this article have been paid for by the Royal Society of Chemistry

Phenothiazine-based TADF emitters with dual conformations for single-molecule white OLEDs

Pavithra V. Prabhu,[ab] Vibhu Darshan,[bc] Indira S. Divya,[ab] Moumita Banerjee,[d] Sunil Varughese,[ab] Anakuthil Anoop,*[e] K. N. Narayanan Unni *[bc] and Joshy Joseph *[ab]

Donor–π–acceptor (D–π–A) type phenothiazine derivatives, exhibiting quasi-axial and quasi-equatorial conformers with distinct photophysical properties, serve as tunable, multifunctional materials for applications in sensors and optoelectronic devices. Herein, we report two phenothiazine based D–π–A emitters, **NTPH** and **NTPCF**, incorporating phenothiazine as the donor and nicotinonitrile as the acceptor, designed as stimuli-responsive functional materials with switchable conformers exhibiting differential optical properties. Single-crystal analyses show that phenothiazine adopts a quasi-axial conformation in **NTPCF**, while **NTPH** exhibits polymorphism with quasi-axial (**NTPH-B**) and quasi-equatorial (**NTPH-O**) conformers. The quasi-axial conformer of **NTPCF** exhibits green emission with a fluorescence maximum at 545 nm, while **NTPH** shows cyan emission with a fluorescence maximum at 463 nm and a shoulder band at around 516 nm. The equatorial conformer of **NTPH** has a characteristic TADF orange emission with a maximum of 585 nm. Theoretical studies highlight that singlet-triplet energy gap ΔE_{ST} is significantly influenced by the molecular conformation and the low energy barriers (<3 kcal mol^{-1}) between the axial and equatorial conformers enable dynamic conformational flexibility at room temperature. Mechano-responsive changes in the emission spectra further support the availability of energetically close, quasi-axial and quasi-equatorial conformers, enabling the tuning of TADF in the solid state. **NTPCF** shows high-contrast, reversible cyan-to-orange mechanochromism ($\Delta\lambda_{em} \sim 135$ nm), suitable for anticounterfeiting, while **NTPH** exhibits irreversible blue-to-orange switching. Solution-processed orange organic light-emitting diodes (OLEDs) based on the neat film of **NTPCF** achieve a high luminance of 8400 cd m^{-2}. Additionally, **NTPCF**-based single-molecule white OLEDs were developed by varying the doping concentration, yielding a cool white OLED with CIE coordinates of (0.33, 0.37), a CRI of 70, and an EQE of 3.36% and a warm white OLED with CIE coordinates of (0.39, 0.45) and an EQE of 4.25%.

Received 14th June 2025
Accepted 18th November 2025

DOI: 10.1039/d5sc04370k

rsc.li/chemical-science

Introduction

Organic light-emitting diodes (OLEDs) have transformed display and lighting technologies owing to their high efficiency, mechanical flexibility, and tunable emission properties. Among the various strategies to improve OLED performance, thermally activated delayed fluorescence (TADF) has emerged as a promising mechanism.[1–3] TADF enables the utilization of both singlet and triplet excitons for light emission *via* reverse intersystem crossing (RISC), achieving near-unity internal quantum efficiencies without relying on heavy-metal-based phosphors.[4–9] Recent TADF emitters further expand this concept by employing multiple-resonance frameworks, higher-lying excited states, and through-space charge transfer designs, simultaneously enabling high efficiency, color purity, and device stability.[10–15] Traditionally, TADF emitters are designed to emit from a single emissive state, typically the lowest singlet excited state (S_1). However, recent advances have focused on the development of dual-emission TADF materials, compounds capable of emitting from two distinct excited states, such as locally excited (LE) and charge-transfer (CT) states, or exhibiting both fluorescence and room-temperature phosphorescence (RTP).[16,17] Incorporating dual emission within a single TADF emitter holds the potential for achieving richer emission profiles, broader color tunability, and even single-molecule white-light emission.[18,19] This capability is particularly promising for the design of color-tunable OLEDs and the development of simplified white OLEDs,

[a]*Chemical Sciences & Technology Division (CSTD), CSIR-National Institute for Interdisciplinary Science & Technology, CSIR-NIIST, Thiruvananthapuram, Kerala 695019, India. E-mail: joshy@niist.res.in*

[b]*Academy of Scientific and Innovative Research (AcSIR), Ghaziabad 201002, India*

[c]*Centre for Sustainable Energy Technologies (C-SET), CSIR-NIIST, Thiruvananthapuram, Kerala 695019, India. E-mail: unni@niist.res.in*

[d]*Department of Chemistry, Indian Institute of Technology, Kharagpur, India*

[e]*School of Digital Sciences, Kerala University of Digital Sciences, Innovation, and Technology, Thiruvananthapuram, Kerala, India. E-mail: anoop.a@duk.ac.in*

offering potential advantages in terms of device architecture, color stability, and cost efficiency.[20,21]

In recent years, stimuli-responsive TADF materials have gained significant attention due to their unique ability to modulate emission properties in response to external stimuli such as temperature,[22] UV irradiation,[23] mechanical force like grinding,[24–28] and solvent polarity.[29] These materials hold great promise for applications in sensing, imaging and anti-counterfeiting technologies.[30] Recent studies have identified several molecules that integrate TADF and mechanochromism, displaying distinct luminescence colour changes under mechanical stress like grinding and shearing.[31–33] These stimuli-induced modifications can alter molecular conformations, excited-state ordering, or singlet-triplet energy gap (ΔE_{ST}) and may enable partial violation of Kasha's rule by facilitating radiative transitions from multiple excited states. This approach helps in the tuning of TADF and opens pathways for smart, tunable luminescent materials.

A particularly promising application of dual-emission TADF materials is the realization of white-light emission from a single molecular emitter.[34–36] Generally, white OLEDs rely on multiple emissive layers or dopants emitting in complementary spectral regions (typically blue, green, and red), which increases fabrication complexity and often results in color instability over time.[37] In contrast, single-component white emitters offer significant advantages, including simplified device architecture, improved color stability, and better color balance.[38,39] Achieving such functionality requires careful molecular design to balance radiative decay from different states, ensure efficient RISC, and maintain high photoluminescence quantum yields (PLQYs) under device operating conditions. While photoluminescent white light emission has been successfully demonstrated in many cases, achieving efficient electroluminescence (EL) from these materials continues to be a major challenge.[18,40–42]

Recent studies have demonstrated that TADF molecules with twisted donor–acceptor (D–A) architectures can exhibit dual emission *via* simultaneous population of CT and LE states, which is usually aided by conformational heterogeneity.[32,43,44] Among various twisted donor motifs, phenothiazine has attracted significant attention due to its non-planar, butterfly-shaped structure, which imparts inherent conformational flexibility and strong electron-donating ability.[45–51] This flexibility gives rise to quasi-axial and quasi-equatorial conformers, whose coexistence significantly influences photophysical behavior.[36,52] Exploiting this conformational duality, phenothiazine-based emitters have also been employed as single-component white-light emitters for OLED applications. Although phenothiazine derivatives have been explored for white-light emission, their application in single-molecule white organic light-emitting diodes (WOLEDs) remains relatively limited, with only a few reported examples to date.[43,44,53–55]

Not all phenothiazine motifs with conformational flexibility are capable of producing white-light emission.[56,57] Only those engineered with well-separated and balanced emissive processes, often through dual conformers or combined fluorescence/TADF or fluorescence/RTP, can achieve white emission.[58] Without such carefully optimized structural and photophysical features, these flexible molecules typically yield single-color emission or insufficiently complementary dual emission.[49,59,60] In this context, careful molecular design of phenothiazine-based emitters is important. By adjusting donor–acceptor orientation, controlling the balance of conformers, and choosing suitable host environments, their excited-state behavior can be tuned. These approaches can enable the development of efficient single-molecule WOLEDs and help clarify how the molecular structure affects the emission properties of flexible luminophores.

Herein, we present two strategically designed phenothiazine-based fluorophores, **NTPH** and **NTPCF**, structurally well-defined D–π–A molecules featuring phenothiazine as the electron donor and a nicotinonitrile unit bearing two phenyl groups as the electron acceptor. In **NTPCF**, a trifluoromethyl ($-CF_3$) group was introduced to enhance the electron-withdrawing ability of the acceptor, thereby fine-tuning its electronic characteristics. Nicotinonitrile derivatives are well known for their excellent electron-transporting and hole-blocking properties, making them highly suitable for OLED applications.[61] The incorporation of a phenyl π-bridging spacer offers optimal separation between the donor and acceptor units, enabling facile bond rotation that limits spatial orbital overlap, thereby resulting in a small ΔE_{ST}. Furthermore, single-crystal X-ray diffraction (SCXRD) studies enabled the identification of two distinct conformers of **NTPH**, providing key insights into the role of molecular packing and intermolecular interactions in modulating luminescence changes and the reversible TADF "on–off" switching upon mechanical stimulation (grinding). Notably, **NTPCF** exhibited high-contrast, reversible mechanochromism, demonstrating potential utility in anticounterfeiting applications. Furthermore, solution-processed OLEDs based on neat films of **NTPH** and **NTPCF** without any host were successfully fabricated, and additionally, warm and cool white OLEDs were realized using **NTPCF** by carefully tuning the doping concentration. These findings represent a compelling direction for multifunctional OLED platforms that integrate stimuli-responsive photophysics, TADF, and dual emission in a single-component system.

Results and discussion

Design and synthesis

N-Phenyl substituted phenothiazine derivatives are known to exhibit polymorphism featuring quasi-axial, quasi-equatorial and intermediate conformers.[62] These conformers differ in the degree of planarization of the phenothiazine ring and in the dihedral angle between the phenothiazine core and the attached phenyl ring.[63,64] The nature of the *N*-substituents significantly influences the conformer population, crystal packing, and the resulting photophysical properties.[60,65] Quasi-axial conformers, characterized by a puckered phenothiazine ring, possess an excited singlet state with dominant LE character and typically emit in the short-wavelength region.[66] In contrast, quasi-equatorial conformers, having a nearly planar phenothiazine ring and an orthogonal *N*-phenyl substituent, exhibit significant CT character in their lower excited states with

very low ΔE_{ST}, leading to emission at longer wavelengths, either *via* RTP or TADF.[49] In D–π–A type phenothiazine derivatives, the strength of the acceptor group can modulate the conformer population, crystal packing and excited state energy levels, resulting in switchable conformers with distinct physical and optical characteristics. In this study, we have designed two such derivatives, **NTPH** and **NTPCF**, incorporating phenothiazine as the donor, a nicotinonitrile core bearing two phenyl substituents as the acceptor and a phenyl group serving as the π-bridge (Fig. 1). The acceptor strength is tuned by incorporating an electron withdrawing $-CF_3$ group on one of the phenyl substituents on nicotinonitrile in **NTPCF**, which will stabilize the excited state energy levels and alter the optical properties, without significantly perturbing the overall molecular geometry.

The target molecules, **NTPH** and **NTPCF**, were synthesized *via* following modified procedures, as outlined in the synthetic routes shown in Scheme S1. The key step involves a Buchwald–Hartwig coupling between phenothiazine and the synthetic intermediates **NTH-Br** or **NTCF-Br**, yielding the target compounds, **NTPH** and **NTPCF**, with yields exceeding 65%. The chemical structures of both molecules were characterized and confirmed *via* ^{1}H NMR, ^{13}C NMR, and high-resolution mass spectrometry (HRMS) (Fig. S1–S6). Additionally, their molecular structures were unambiguously determined by single-crystal X-ray crystallography (Fig. 1).

Thermal and electrochemical properties

The thermal properties of the molecules were studied by thermogravimetric analysis (TGA) and differential scanning calorimetry (DSC) under a nitrogen atmosphere (Fig. S7). Both **NTPH** and **NTPCF** exhibited good thermal stability, with decomposition temperatures corresponding to a 5% weight loss observed at 326 °C and 312 °C, respectively. DSC measurements of the powdered samples were conducted over a temperature range of 30 °C to 280 °C to explore thermal transitions. The pristine powders of **NTPH** and **NTPCF** displayed prominent endothermic peaks at 215 °C and 240 °C, respectively, corresponding to their melting points. Notably, for **NTPH**, an additional exothermic peak at 144 °C and an endothermic peak at 154 °C were detected prior to melting, suggesting a possible phase transition to a more stable form which is an indication of polymorphism.

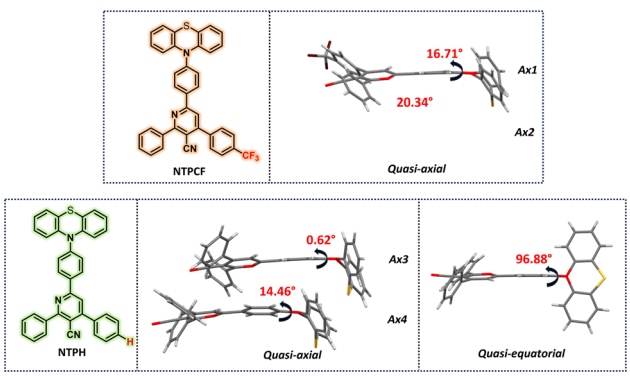

Fig. 1 Molecular structures of the synthesized molecules and molecular conformations of corresponding single crystals.

The frontier molecular orbital energies (HOMO and LUMO) of **NTPH** and **NTPCF** were estimated using cyclic voltammetry (CV). As illustrated in Fig. S8, both compounds exhibited a one-electron redox process in chlorobenzene solution, attributed to the oxidation of the phenothiazine donor unit and the reduction of the nicotinonitrile unit. The HOMO energy levels were determined from the onset oxidation value of the cyclic voltammogram, while the LUMO levels were calculated using the HOMO values and the optical bandgap. The calculated HOMO/LUMO energy levels were −5.08 eV/−2.10 eV for **NTPH** and −4.80 eV/−1.85 eV for **NTPCF**. The slightly lower HOMO and LUMO energies in **NTPCF** are attributed to the presence of the strong electron-withdrawing $-CF_3$ group in the acceptor unit.

Theoretical investigations

To investigate the conformational flexibility and steric interactions within the donor-phenyl spacer segment of **NTPH** and **NTPCF**, relaxed ground state potential energy surface (PES) scans were performed in the gaseous phase. The PES scan involved rotation about the dihedral angle between the phenyl spacer and the phenothiazine donor unit. All calculations were done using the B3LYP/def2-TZVP level of theory,[67–71] incorporating D3BJ dispersion corrections[72] with RIJCOSX[73] and performed using the ORCA 5.0.3 software package.[74] The singlet (S_1) and triplet (T_1) energies were calculated as adiabatic (relaxed) excitation energies obtained from geometry optimizations of the respective excited states, and the energy difference between them was denoted as ΔE_{ST}. The computed geometrical parameters (bond lengths, bond angles, and dihedral angles) are presented in Table S6 (SI II) and have been compared with the single-crystal XRD data. The computed results show good agreement with the experimental parameters, confirming their reliability.

The ground-state rotational energy profiles of **NTPH** and **NTPCF** from PES scan (Fig. 2A and B) provide quantitative insight into the torsional flexibility of the donor-phenyl spacer linkage. The computed profiles exhibit two nearly symmetric minima at dihedral angles of approximately 90° and 270°, corresponding to quasi-equatorial (orthogonal) conformations, and two maxima near 0° and 180°, representing quasi-axial (planar) geometry. The barrier heights separating these conformers are modest, approximately 2.8 kcal mol^{-1} for **NTPH** and 3.1 kcal mol^{-1} for **NTPCF**, indicating facile interconversion at room temperature.

Along the rotation coordinate, the degree of conjugation between the donor and spacer changes continuously. In planar geometries (0° and 180°), strong π-conjugation between phenothiazine and the phenyl ring promotes orbital delocalization and a large HOMO–LUMO overlap, yielding higher ΔE_{ST} values (>0.5 eV). As the torsion increases toward 90° and 270°, the donor and spacer π-planes become nearly orthogonal, suppressing electronic coupling and forming a twisted intramolecular charge-transfer (TICT) configuration. This decoupling reduces the exchange interaction, leading to small ΔE_{ST} values (~0.02–0.05 eV). The DFT-derived rotation profiles clearly delineate how conformational motion governs the electronic coupling and photophysical response in these donor–acceptor systems.

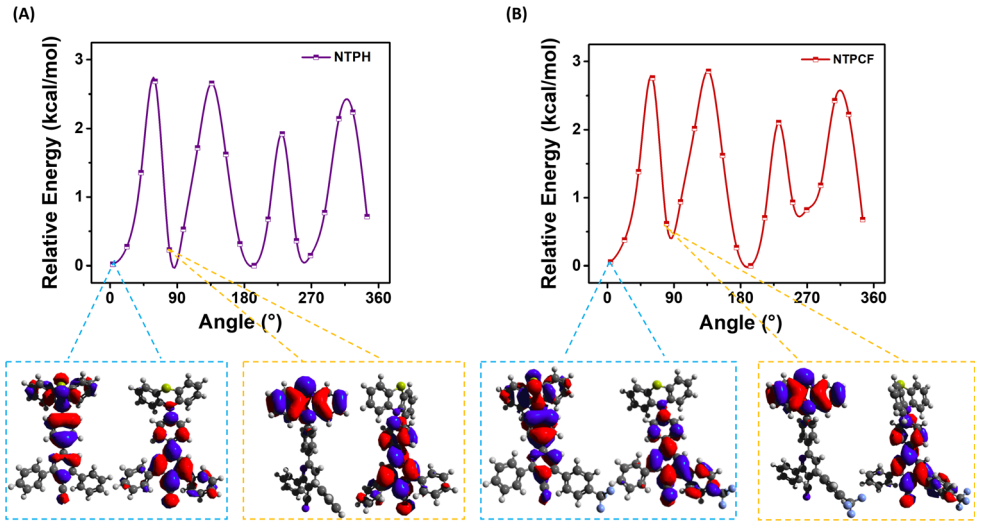

Fig. 2 Relaxed PES scan of the ground state (gas phase) as a function of the twist angle between the phenyl spacer and the phenothiazine unit of (A) **NTPH** and (B) **NTPCF**. The HOMO and LUMO of quasi-equatorial (orange box) and quasi-axial (blue box) are also given.

The frontier molecular orbitals (HOMO and LUMO) of both conformations of **NTPH** and **NTPCF** were visualized to investigate their electronic structures and charge-transfer characteristics. The corresponding molecular orbital plots for both conformers of **NTPH** and **NTPCF** are presented in Fig. 2. In the axial conformations of both molecules, the HOMO and LUMO exhibit considerable spatial overlap, resulting in a larger ΔE_{ST}. In contrast, the quasi-equatorial conformations display a spatial separation between the frontier orbitals with the HOMO localized on the phenothiazine donor moiety and LUMO distributed across the nicotinonitrile acceptor unit. This spatial separation of electron density between the HOMO and LUMO confirms significant intramolecular charge-transfer (ICT) character, which is desirable for TADF behavior as it leads to a reduction in exchange energy and hence a smaller ΔE_{ST}.

Additionally, we computed the variation in ΔE_{ST} for each relaxed geometry along the ground-state PES scan, with the values plotted as a function of the donor–acceptor dihedral angle (Fig. 3A and B). Higher ΔE_{ST} values (>0.6 eV) were observed in the quasi-axial conformations, indicating stronger orbital overlap and reduced charge-transfer character. In contrast, for both **NTPH** and **NTPCF**, the minimum ΔE_{ST} values occur at near dihedral angles of approximately 90° and 270°, corresponding to twisted (quasi-equatorial) conformations, identified as global minima on the relaxed PES. At these twisted geometries, ΔE_{ST} approaches near-zero values (~0.02–0.05 eV) in both systems. These results clearly demonstrate that conformational control is crucial for tuning ΔE_{ST} and that twisted geometries are essential for enabling efficient TADF. Furthermore, the excitation energies of the singlet and triplet states for the quasi-equatorial conformers of **NTPH** and **NTPCF** are shown in Fig. 3C. For **NTPH**, the S_1 and T_1 energies are 2.195 and 2.189 eV, respectively, yielding a small ΔE_{ST} of 0.006 eV. Similarly, for **NTPCF**, the S_1 and T_1 energies are 2.062 and 2.057 eV, resulting in a ΔE_{ST} of 0.005 eV. In comparison, the estimated ΔE_{ST} values for the quasi-axial conformations are significantly higher, calculated to be 0.59 eV for **NTPH** and 0.53 eV for **NTPCF**. To further confirm the TADF characteristic of the molecule we recalculated the lowest singlet and triplet excited-state energies in implicit toluene (CPCM) at the same level of theory as in the gas phase. The singlet–triplet gaps remain near zero in the toluene solvent phase also: for **NTPH**, S_1 = 2.195 eV, T_1 = 2.189 eV, and ΔE_{ST} = 0.006 eV and for **NTPCF**, S_1 = 2.062 eV, T_1 = 2.057 eV, and ΔE_{ST} = 0.005 eV. These results further confirm that twisted quasi-equatorial geometries are highly favorable for TADF performance due to their minimal singlet–triplet energy gaps.

Single crystal analyses

To elucidate the structure–property relationships, we performed an in-depth analysis of SCXRD data, providing detailed insights into molecular packing, conformation, and intermolecular

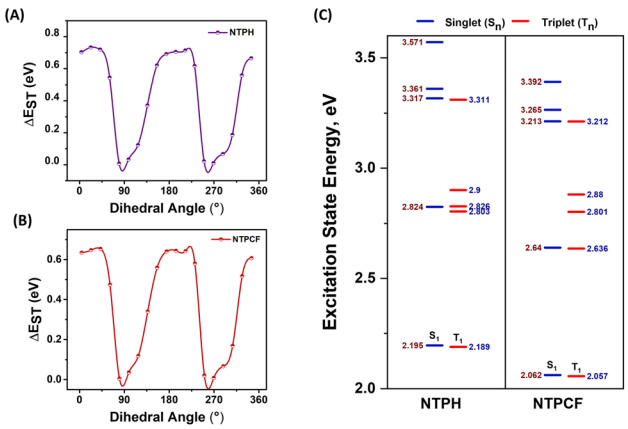

Fig. 3 Calculated ΔE_{ST} for each conformer obtained from the relaxed potential energy surface scan on the ground state (gas phase) (A) **NTPH** and (B) **NTPCF**. Singlet and triplet state energies of **NTPH** and **NTPCF** for quasi-equatorial conformation (C). Calculations were done using TDDFT at the B3LYP/def2-TZVP-D3BJ level of theory.

interactions within the crystal lattice. The crystallographic data for NTPCF (Table S1), NTPH-B (Table S2), and NTPH-O (Table S3) are included in the SI I. The ORTEP diagrams of **NTPCF** and **NTPH** are given in Fig. S9. Green-emissive, needle-like single crystals of **NTPCF** were obtained *via* slow evaporation of its toluene solution, crystallizing in the triclinic system with space group $P1$ with $Z = 4$. Notably, the unit cell of **NTPCF** consists of two twinned axial crystal pairs, each containing two asymmetric units, *Ax1* and *Ax2*, interconnected by intermolecular interactions forming a dimeric unit (Fig. S10). In both *Ax1* and *Ax2*, phenothiazine adopts a quasi-axial conformation, with its central sulphur- and nitrogen-containing ring assuming a boat-like conformation. The torsional angles between the phenothiazine and the benzene ring are 16.71° and 20.34° for *Ax1* and *Ax2*, respectively. The *Ax1*–*Ax2* dimer structure reveals a network of non-covalent interactions including π–π, C–H···π, C–H···N, C–S and C–N interactions, that contribute to its molecular stability and packing arrangement. A detailed analysis and discussion of these interactions are provided in the SI (Fig. S10). Along the *a*-axis, the molecules adopt a head-to-head arrangement, while along the *c*-axis, they form a slip-stacked head-to-tail configuration that helps minimize steric hindrance (Fig. S11). The columns aligned along the *a*-axis are interconnected through C–H···F interactions (2.77–2.95 Å) and π–π stacking (3.58 and 3.67 Å), leading to interdigitated layers and the formation of a corrugated, sheet-like structure.

Slow evaporation of **NTPH** solution in a 4 : 2 : 1 mixture of dichloromethane, ethyl acetate and acetonitrile yielded two **NTPH** polymorphs: cyan emissive, needle-like crystals (referred to as **NTPH-B**) and orange emissive, plate-like crystals (referred to as **NTPH-O**) (Fig. 4). **NTPH-B** crystallizes in the triclinic system with space group $P1$ and $Z = 4$. It corresponds to the quasi-axial conformer of phenothiazine, adopting a conformation similar to that observed in the green-emissive **NTPCF** crystals. The structure has two twinned axial conformers, denoted as *Ax3* and *Ax4*, which together form an asymmetrical dimer unit. *Ax3* exhibits a nearly zero twist angle between the phenothiazine and the phenyl spacer, whereas *Ax4* shows a torsional angle of 14.35°. As shown in Fig. 4A and B, the interface between the symmetric equivalents, *Ax2* and *Ax3*, of **NTPH-B** adopts a head-to-head parallel arrangement, stabilized by multiple C–H···π interactions (2.77–3.51 Å) and π–π stacking interactions (3.49, 3.65, and 3.63 Å). An internal pore is formed through the antiparallel packing of the asymmetric units *Ax3* and *Ax4*, facilitated by additional C–H···π interactions (2.99 Å, 3.10 Å and 3.18 Å) (Fig. 4C). This packing arrangement generates a long-range, orderly channel structure, resulting in the formation of slipped, 2D corrugated layers (Fig. S12).

NTPH-O crystallizes in the monoclinic system with space group $P2_1/c$ and $Z = 4$. It corresponds to the quasi-equatorial conformer of phenothiazine, in which the phenothiazine adopts a planar orthogonal conformation, with a torsional angle of 96.88° relative to the phenyl spacer. Unlike **NTPH-B**, no asymmetric unit is observed in the unit cell. As shown in Fig. 4E and S13, the molecules in **NTPH-O** adopt a head-to-tail, slip-stacked antiparallel arrangement, resulting in a tightly packed two-dimensional sheet-like structure. This packing is stabilized by multiple intermolecular interactions (Fig. 4D and F), including C–H···π interactions (2.99–3.20 Å). Strong π–π stacking interactions are observed between the phenothiazine and the phenyl rings attached to the nicotinonitrile group (3.46 Å, 3.60 Å, and 3.44 Å). Additionally, a C–H···S interaction (3.04 Å) connects the phenothiazine and the phenyl ring, further reinforcing the head-to-tail configuration. A C–H···N

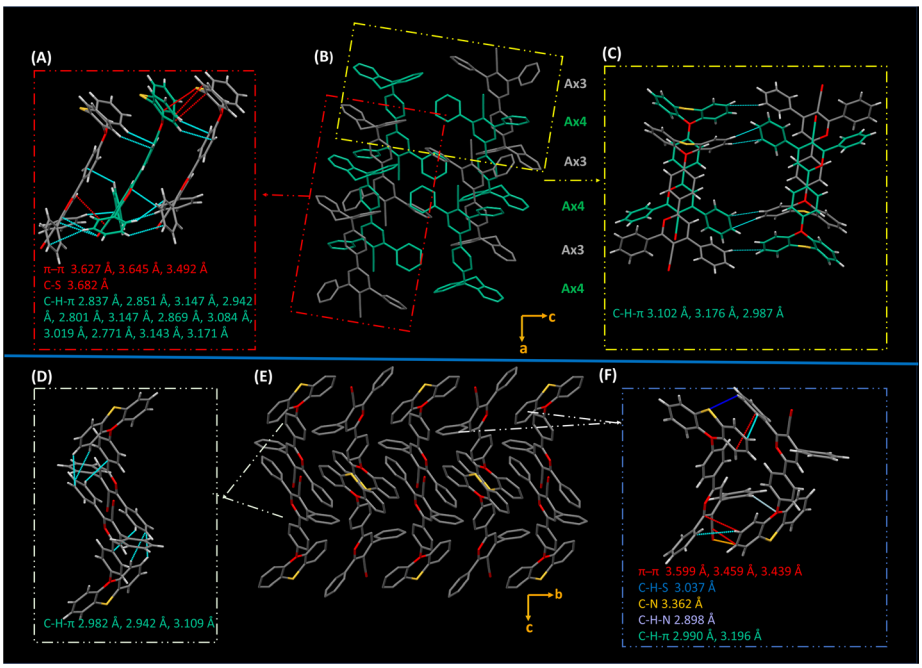

Fig. 4 The crystal packing mode of (B) **NTPH-B** and (E) **NTPH-O**. The interactions between (A) axial pairs, Ax3 and Ax4 and (C) two columns of **NTPH-B**. The interactions between equatorial pairs (D) along the *c* axis and (F) along the *b* axis of **NTPH-O**.

interaction (2.90 Å) between the phenothiazine and a phenyl hydrogen also contributes to the overall structural stability. The distinct packing patterns observed highlight the crucial role of molecular conformation in modulating spatial arrangements, determining crystal packing motifs, and influencing the photophysical and optical properties of the materials.

Solution state photophysical studies

The UV-Vis absorption and steady-state photoluminescence (PL) spectra of **NTPCF** and **NTPH** were recorded in dilute toluene solutions (1×10^{-5} M) at room temperature (Fig. 5A), and key photophysical parameters are summarized in Table S4. The absorption spectra of both compounds display a strong π–π* transition near 300 nm and a broad CT band at around 370 nm. In the PL spectra, both **NTPCF** and **NTPH** exhibit dual emission. **NTPH** shows emission peaks at 420 nm (LE) and 580 nm (CT), while **NTPCF** exhibits corresponding red-shifted peaks at 440 nm and 608 nm, respectively. The higher-energy LE band is attributed to the quasi-axial conformation of the phenothiazine donor, exhibiting weak CT character, whereas the lower-energy emission corresponds to the quasi-equatorial conformation with a strong CT nature. These assignments are consistent with theoretical predictions, solvatochromic studies (Fig. S14) and previous reports on similar phenothiazine-based donor–acceptor systems and are further supported by our single-crystal structural analyses.[75,76]

The quasi-equatorial conformations of phenothiazine-based donor–acceptor systems with strong excited state CT character are known to exhibit delayed fluorescence *via* a TADF mechanism.[54] Our theoretical calculations on **NTPCF** and **NTPH** predicted near zero ΔE_{ST} values for both derivatives (0.006 eV and 0.005 eV, respectively) in the quasi-equatorial conformers. To confirm the involvement of possible TADF, steady-state PL spectra of **NTPCF** (Fig. 5B) and **NTPH** (Fig. S15A) were recorded in dilute toluene solutions (1×10^{-5} M) under both argon and oxygen saturated conditions. For both molecules, a significant quenching of long-wavelength emission was observed in the presence of oxygen, suggesting the involvement of triplet excited states in the emission process. Transient PL decay measurements were carried out under argon and oxygen atmospheres to further investigate the TADF nature. As shown in Fig. 5C, **NTPCF** exhibits a biexponential decay at 600 nm with a prompt component of 15 ns and a delayed component of 521 ns.

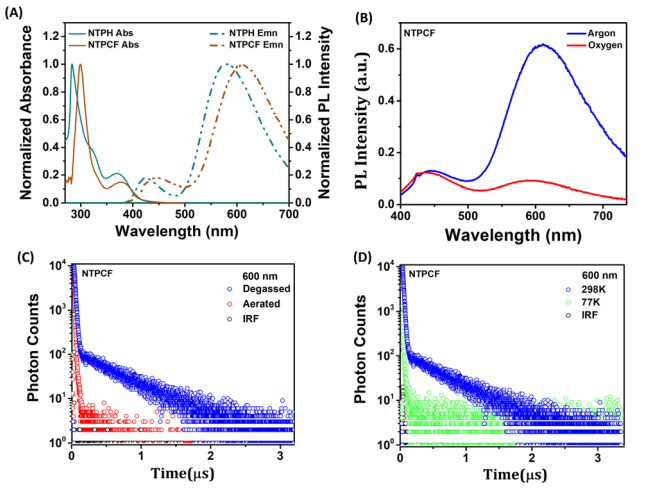

Fig. 5 (A) Normalized UV/visible absorption spectra and steady-state PL spectra measured in toluene solution (1×10^{-5} M) at room temperature of NTPH and NTPCF and (B) steady state PL spectra of NTPCF in toluene under argon and oxygen saturated conditions. The transient PL decay profiles of NTPCF in toluene solutions probed at 600 nm, (C) under aerated and degassed conditions and (D) at 77 K and 298 K.

Similarly, **NTPH** displays biexponential decay at 580 nm with prompt and delayed lifetimes of 16 ns and 558 ns, respectively (Fig. S15B). In the presence of oxygen, both molecules show complete suppression of the delayed component, confirming that the long-wavelength emission arises from TADF. In contrast, transient PL decay at shorter wavelengths reveals only prompt fluorescence, indicating that TADF is specifically associated with the quasi-equatorial conformation, responsible for long-wavelength emission and the corresponding lifetime values are provided in Table S5. Further evidence for TADF was obtained from temperature-dependent transient PL studies at 77 K and 300 K (Fig. 5D and S15C), which demonstrated an increase in delayed emission with rising temperature, consistent with the thermally activated nature of the delayed fluorescence in both emitters.

The phosphorescence spectra of **NTPCF** and **NTPH** were recorded in toluene glass at 77 K and compared with their fluorescence in dilute toluene solutions at 298 K (Fig. S16A and B). Interestingly, both molecules exhibited phosphorescence originating from a localized ^{3}LE state, which was blue-shifted relative to the long wavelength TADF emission assigned to the quasi-equatorial conformer. Notably, the emission from the ^{3}CT state corresponding to the quasi-equatorial band was absent at 77 K, likely due to restricted molecular rotations in the frozen toluene matrix. Similar observations were previously reported for phenothiazine-based donor–acceptor systems, supporting the involvement of a localized ^{3}LE state at lower temperatures.[77,78] At elevated temperatures, increased conformational flexibility facilitates the formation of quasi-equatorial conformers, leading to red-shifted emissions from the ^{1}CT/^{3}CT states. To further probe the nature of the ^{3}LE emission, we compared the phosphorescence spectra of **NTPCF** in toluene and in relatively polar 2-methyltetrahydrofuran (2-MeTHF) at 77 K (Fig. S17A). Minimal solvent dependence was observed, reinforcing the localized nature of the ^{3}LE state. Additionally, the phosphorescence spectrum of the isolated acceptor moiety, measured under identical conditions (Fig. S17B), closely matched that of **NTPCF** in both emission maxima and spectral profile. This spectral overlap strongly suggests that the observed triplet emission in **NTPCF** arises predominantly from a ^{3}LE state localized on the acceptor unit.

Based on the onset of phosphorescence, the ^{3}LE state energies for **NTPH** and **NTPCF** were estimated to be 2.56 eV and 2.63 eV, respectively. From spectroscopic measurements, the ^{1}LE (quasi-axial) and ^{1}CT (quasi-equatorial) states were estimated to be 3.15 eV and 2.47 eV for **NTPH** and 3.10 eV and 2.40 eV for **NTPCF**,

respectively. In the quasi-axial conformation, due to puckering, the nitrogen lone pair exhibits reduced localization into the phenyl rings of phenothiazine, resulting in significant HOMO–LUMO overlap (Fig. 2) and enhanced D–A conjugation. This leads to a higher singlet–triplet separation with reduced charge separation. In contrast, the quasi-equatorial conformation with more planar phenothiazine rings allows greater delocalization of the nitrogen lone pair, decreasing HOMO–LUMO overlap and D–A conjugation. This promotes electronic decoupling in quasi-equatorial conformers and facilitates a lower-energy CT state with more efficient charge transfer. Accordingly, the energy difference between the ^{1}LE and ^{3}LE states (denoted as $\Delta E_{ST,ax}$) for **NTPH** and **NTPCF** was estimated to be 0.63 and 0.51 eV, respectively, in good agreement with the TD-DFT calculations (0.59 eV & 0.53 eV). Since the ^{3}CT emission associated with the quasi-equatorial conformer was not detected under these conditions, experimental determination of the corresponding ΔE_{ST} values was not feasible. Therefore, we relied on values derived from TD-DFT calculations.

Solid state luminescence & mechanochromism

Due to the dual-conformation flexibility of the phenothiazine moiety, both emitters exhibited stimulus-responsive fluorescence with high contrast and sensitivity. Based on this structural feature, we investigated the mechanochromic behaviour of **NTPH** and **NTPCF** in detail. The pristine powder samples of both compounds were obtained by precipitation from dichloromethane and hexane, while the single crystals were prepared as discussed in the previous section. For **NTPCF**, the pristine powder displayed a broad cyan emission with a maximum at 457 nm, while its single crystal exhibited a red-shifted green emission at 545 nm (Fig. 6A and S18). Upon mechanical grinding of the pristine powder (Fig. 6A and C), the emission further red shifted to orange, with a maximum at 593 nm. The original cyan fluorescence was restored upon fuming with solvent vapors, such as chloroform, dichloromethane or hexane. This fluorescence colour change was reversible and repeatable over multiple cycles.

In the case of **NTPH**, the pristine powder showed dual-emission bands with peaks at 463 nm and 516 nm. Mechanical stimuli induced a red shift of the emission maximum to around 585 nm (Fig. 6D and F). Fuming the ground sample of **NTPH** with chloroform, even for five minutes, couldn't completely reverse the emission of the pristine powder and lead to a very broad emission covering the entire visible region. Among the single crystal polymorphs, **NTPH-B** exhibited bluish-green emission with dual peaks at 467 nm and 510 nm, whereas **NTPH-O** emitted an orange fluorescence centered at 585 nm (Fig. 7). Interestingly, the emission profile of **NTPH-B** matched that of the pristine powder, while **NTPH-O** mirrored the emission of the ground sample, establishing a clear correlation between mechanochromic behavior and molecular conformation. As illustrated in Fig. 7 and discussed earlier, we can assign that the higher energy bluish-green emission originates from the LE state (quasi axial conformer), while the orange emission band originates from the CT state (quasi-equatorial conformer). Furthermore, the computational studies predicted lower energy barriers between the conformers (<3 kcal mol^{-1}), indicating good conformational flexibility at room temperature. These results underscore the critical role of conformational flexibility in modulating photophysical responses to mechanical stimuli.

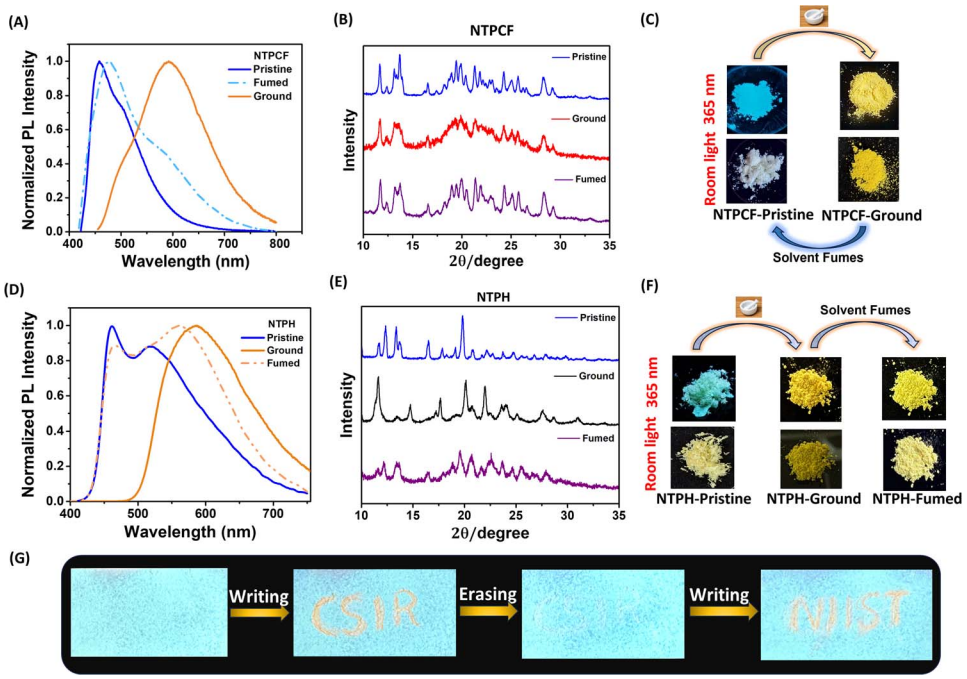

Fig. 6 Normalized emission spectra and photographs under UV excitation of (A and C) **NTPCF** and (D and F) **NTPH** in different solid-states. PXRD patterns of pristine, ground and fumed samples of (B) **NTPCF** and (E) **NTPH** and (G) demonstration of rewritable mechanochromism: photographs, under UV light showing, writing and erasing *via* solvent fuming on a filter paper coated with **NTPCF**.

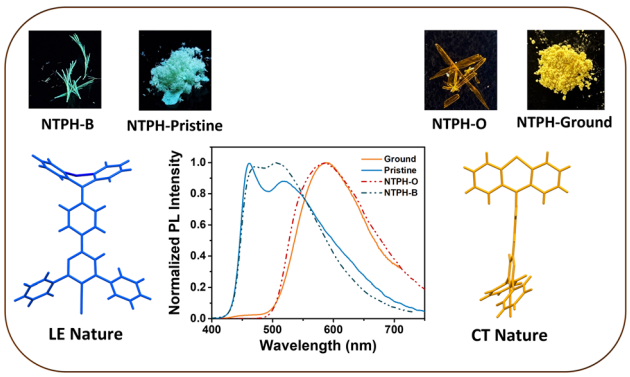

Fig. 7 Schematic figure illustrating the correlation between the mechanochromic behaviour and molecular conformation of NTPH.

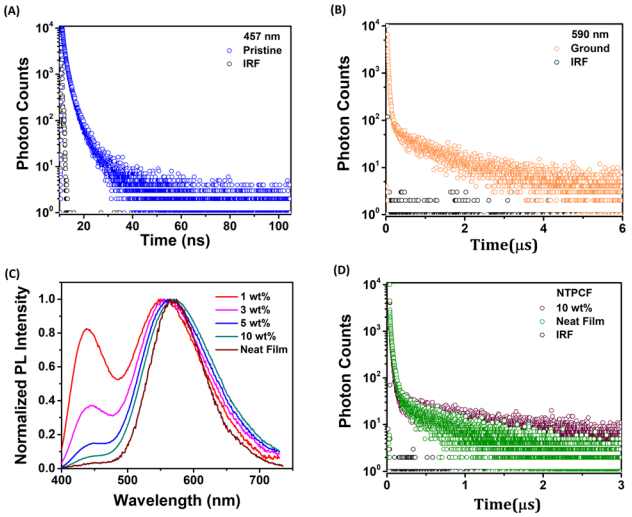

Fig. 8 Transient PL decay spectra of NTPCF (A) before and (B) after mechanical grinding. (C) Steady-state PL spectra of films of PVK doped with varying concentrations of NTPCF (1 wt%, 3 wt%, 5 wt% and 10 wt% and neat), excited at 375 nm. (D) Transient PL decay spectra of NTPCF in the film state; comparison between the neat film and 10 wt% PVK-doped samples.

To further understand the photoluminescence characteristics, absolute photoluminescence quantum yield (PLQY) measurements were performed before and after grinding. For **NTPCF**, the pristine form exhibited a maximum PLQY of 35%, which decreased to 14% after grinding. In contrast, **NTPH** showed a PLQY of 15% in its pristine form, which increased to 19% after grinding. These results demonstrate that a subtle modification of the acceptor unit, such as introducing a $-CF_3$ group, can significantly enhance the quantum yield and influence mechanochromic response.

To understand the mechanism of the observed mechanochromism, powder X-ray diffraction (PXRD) analyses were performed on the pristine, ground and fumed powders of both derivatives (Fig. 6B and E). The sharp and intense diffraction peaks observed in the pristine powders of **NTPCF** and **NTPH** confirm their crystalline nature. Upon grinding, **NTPCF** showed a significant loss of peak intensity and broadening of the diffraction pattern, indicating a transition to a semi-crystalline state. In contrast, **NTPH** retained its crystallinity even after grinding, with the appearance of new peaks, suggesting a crystalline-to-crystalline transformation. For **NTPCF**, the original crystallinity was fully restored upon fuming the ground sample, as evidenced by the reappearance of sharp diffraction peaks. However, in the case of **NTPH**, only partial recovery of crystallinity was observed after fuming. These observations are in agreement with the observed changes in their optical properties. Furthermore, we have demonstrated the write-erase-rewrite process using **NTPCF** coated filter paper, as shown in Fig. 6G. The high-contrast and reversible mechanochromic behaviour of **NTPCF** highlights its potential for applications in anti-counterfeiting rewritable paper.

Solid-state transient PL decay measurements of **NTPH** (Fig. S19A and B) and **NTPCF** (Fig. 8A and B) were carried out before and after grinding to investigate their excited-state dynamics. Interestingly, the results revealed mechanical stimuli-induced TADF in both emitters, enabling them to perform as TADF on/off systems. In the pristine state, both **NTPH** and **NTPCF** showed only nanosecond lifetimes, corresponding to prompt fluorescence. However, upon mechanical grinding, the PL decay spectra of both emitters displayed two components: a nanosecond-scale prompt component and a microsecond-scale delayed component, consistent with TADF behavior. These delayed components match those observed in the long-wavelength region in toluene solution, and the corresponding lifetime values are provided in Table S5. This TADF activation is accompanied by the transition from the quasi-axial to quasi-equatorial state, thereby promoting efficient RISC and delayed fluorescence.

To understand the excited-state behavior of solution-cast films of **NTPCF** and **NTPH** under conditions relevant to OLED applications, both emitters were incorporated into poly(*N*-vinyl carbazole) (PVK), a widely used OLED host matrix. Steady-state and time-resolved PL measurements were performed at various doping concentrations to evaluate their emission characteristics. At a low doping concentration of 1 wt%, both **NTPCF** (Fig. 8C) and **NTPH** (Fig. S20A) exhibited emission contributions from the axial and equatorial conformers, resulting in white-light emission. However, with increasing doping concentrations, the contribution from the axial conformer gradually diminished. At 10 wt% doping, the emission was predominantly attributed to the equatorial conformation. This shift suggests that increased molecular aggregation at higher concentrations facilitates intermolecular energy transfer from the higher-energy quasi-axial to the lower-energy quasi-equatorial state, thereby altering the overall emission profile.

The transient PL decay profiles of **NTPCF** (Fig. 8D) and **NTPH** (Fig. S20B) were examined in both neat and 10 wt% PVK-doped films. In both cases, prompt (nanosecond scale) and delayed (microsecond scale) emission components were observed (Table S5). Upon doping, the delayed emission component showed a marked enhancement, from 604 ns to 1.1 μs for **NTPCF** and from 551 ns to 1.3 μs for **NTPH**, indicating a significant increase in delayed fluorescence. For 1 wt% PVK-

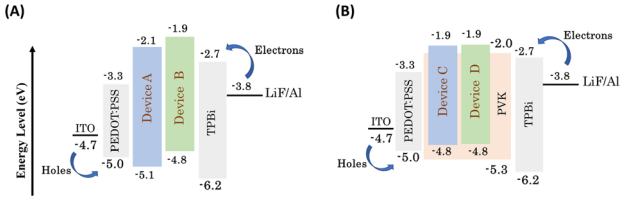

Fig. 9 Schematic diagram of device structure and energy level of OLEDs using (A) **NTPH** (Device A) and **NTPCF** (Device B) neat films and (B) **NTPCF** doped with 1 wt% (Device C) and 10 wt% (Device D) in PVK.

doped **NTPCF**, the axial conformer displayed a maximum emission at 440 nm with a corresponding lifetime of 130 ps (Fig. S21). Collectively, these findings highlight the pivotal role of conformational dynamics, host–guest interactions, and molecular packing in governing the emission behaviour of **NTPCF** and **NTPH** in the film state.

OLED device fabrication

OLED devices were fabricated *via* solution processing using the architectures shown in Fig. 9, employing **NTPH** or **NTPCF** as the emitting layer without a host matrix (Devices A & B). In addition, by utilizing the distinct emission behaviour of **NTPCF** at different doping concentrations in a poly(*N*-vinylcarbazole) (PVK) host matrix, we fabricated cool white and warm white OLEDs (Devices C & D). The corresponding energy level diagrams for all four devices are also shown in Fig. 9. The detailed device structures are as follows: (i) Devices A & B: ITO/PEDOT:PSS (40 nm)/neat **NTPH** or **NTPCF** (30 nm)/TPBi (40 nm)/LiF (1 nm)/Al (100 nm) and (ii) Devices C & D: ITO/PEDOT:PSS (40 nm)/PVK: **NTPCF** (1 wt% for Device C and 10 wt% for Device D) (30 nm)/TPBi (40 nm)/LiF (1 nm)/Al (100 nm). In these configurations, PEDOT:PSS and LiF functioned as the hole- and electron-injection layers, respectively. TPBi served as the electron-transporting and hole-blocking layer, while ITO and Al were used as the anode and cathode electrodes, respectively.

The EL spectra of Device A (neat **NTPH**) and Device B (neat **NTPCF**) are shown in Fig. 10, with EL maxima at 596 nm and 584 nm, respectively. Devices A and B display orange electroluminescence with CIE coordinates of (0.53, 0.46) and (0.52, 0.48), respectively, which can be attributed to the TADF emission from the quasi-equatorial conformation. Device B shows a lower turn-on voltage (V_t: 4 V) compared to Device A (V_t: 5 V). Moreover, Device B (**NTPCF**) outperforms Device A (**NTPH**) in terms of efficiency, achieving a maximum current efficiency (CE) of 5.54 cd A^{-1}, power efficiency (PE) of 2.98 lm W^{-1}, and external quantum efficiency (EQE) of 2.31%, compared to 2.84 cd A^{-1}, 1.49 lm W^{-1}, and 1.39% for Device A. Device B also demonstrates higher luminance, with a maximum value of 8400 cd m^{-2} *versus* 4700 cd m^{-2} for Device A.

To further enhance the performance of **NTPCF** and achieve white OLED emission, PVK was employed as a host matrix at doping concentrations of 1 wt% (Device C) and 10 wt% (Device D). As anticipated, the doped devices exhibited improved EQE, PE, and CE compared to those with neat films of **NTPH** and **NTPCF**. Device C and Device D exhibited dual complimentary emission, as shown in Fig. 11. At 1 wt% doping (Device C), a blue emission peak at 425 nm, attributed to the quasi-axial conformer, was observed alongside the orange emission at 555 nm from the quasi-equatorial conformer. With an increased doping concentration of 10 wt% (Device D), the blue emission intensity diminished while the orange emission became more prominent. The enhancement of orange emission is attributed to the efficient utilization of both singlet and triplet excitons due to the TADF nature of the quasi-equatorial conformer and efficient energy transfer from the quasi-axial conformer, leading to improved device performance.

Device C and Device D both have a turn on voltage of 5 V. Device C achieves a maximum luminance of 2420 cd m^{-2} at a current density of 137 mA cm^{-2}, while Device D reaches 5240

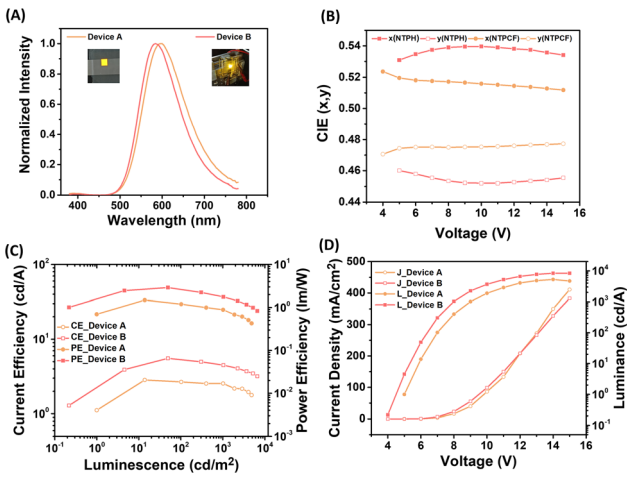

Fig. 10 (A) EL spectra of Devices A and B (inset: the image of real device illumination during operation). (B) CIE *vs.* voltage graph of Devices A and B. (C) Current efficiency–power efficiency–luminance curves of Devices A and B. (D) Current density–voltage–luminance curves of Devices A and B.

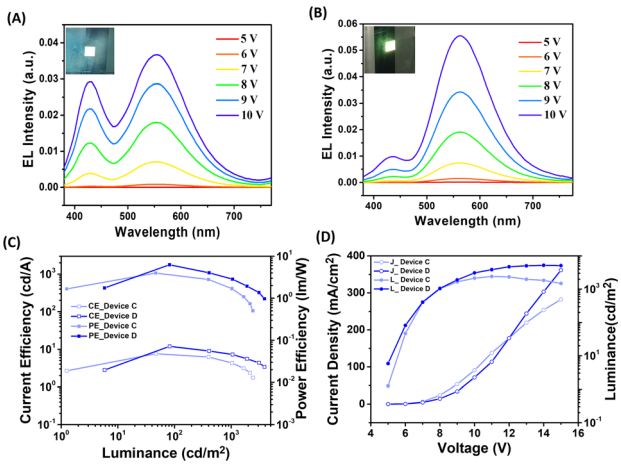

Fig. 11 (A) EL spectra of Device C and (B) Device D (inset: the image of real device illumination during operation). (C) Current efficiency–power efficiency–luminance curves of Device C and Device D. (D) Current density–voltage–luminance curves of Device C and Device D.

cd m^{-2} at 303 mA cm^{-2}. The maximum EQEs are 3.36% for Device C and 4.55% for Device D. Device C delivers a maximum CE of 7.59 cd A^{-1} and PE of 3.97 lm W^{-1}, whereas Device D achieves higher values, with a CE of 11.54 cd A^{-1} and PE of 6.26 lm W^{-1}. At a luminance of 2420 cd m^{-2}, Device C emits cool white light with CIE coordinates of (0.33, 0.37), a correlated color temperature (CCT) of 5740 K, and a color rendering index (CRI) of 70. In contrast, Device D emits warm white light with CIE coordinates of (0.39, 0.45), a CCT of 4040 K, and a CRI of 63 at 3100 cd m^{-2}. Furthermore, at practical brightness levels of 500 cd m^{-2} and 1000 cd m^{-2}, the EQEs of Device C are 2.76% and 1.90%, while Device D achieves EQEs of 3.48% and 2.75%, respectively. Further optimization is currently underway in our lab to enhance the efficiency of the devices.

Conclusion

In summary, we have successfully designed and synthesized two novel donor–acceptor emitters, **NTPH** and **NTPCF**, incorporating phenothiazine as the electron donor and nicotinonitrile as the electron acceptor, linked *via* a phenyl spacer. Single-crystal X-ray diffraction and theoretical calculations confirmed the existence of two conformers, quasi-axial and quasi-equatorial, of the phenothiazine unit. Photophysical studies in both solution and solid states demonstrated dual emission behaviour, with transient PL confirming that the quasi-equatorial conformer exhibits TADF, while the quasi-axial conformer shows prompt fluorescence. Theoretical analysis and crystal packing studies highlighted that molecular conformation and packing significantly influence the ΔE_{ST} and excited-state dynamics. The **NTPH-O** polymorph, characterized by an orthogonal twisted, quasi-equatorial conformation and dense head-to-tail packing, facilitates stronger intramolecular charge transfer (ICT), leading to a reduced ΔE_{ST} and enhanced TADF efficiency. In contrast, the **NTPH-B** polymorph, with its quasi-axial conformation facilitating through-bond π–π interactions, shows weaker ICT and reduced TADF performance. Both emitters exhibited mechanochromic luminescence, with **NTPCF** demonstrating a reversible spectral shift of 135 nm, making it suitable for anti-counterfeiting applications. Both emitters were successfully used to fabricate solution-processed OLEDs with neat films of **NTPCF** and **NTPH**, producing orange electroluminescence, with the **NTPCF**-based device achieving a luminance of 8400 cd m^{-2}. The high PLQY of **NTPCF** also enabled the fabrication of cool and warm white OLEDs by varying the doping concentration in a PVK host matrix. Overall, **NTPH** and **NTPCF** represent promising multifunctional materials for applications in OLEDs and security technologies.

Author contributions

P. V. P. and J. J. conceptualized the work, developed the molecular designs and synthetic protocols and wrote the manuscript. P. V. P. carried out the syntheses, characterization, and photophysical studies of solution, powder and film states. K. N. N. U. and V. D. carried out the device fabrication and optimization. S. V. and I. S. D. helped with single crystal analyses. A. A. and M. B. did the theoretical calculations. All authors reviewed and edited the final manuscript.

Conflicts of interest

There are no conflicts to declare.

Data availability

All supporting data are provided within the article and its accompanying supplementary information (SI). Supplementary information: experimental details, synthetic procedures, structural characterization (NMR, HRMS), theoretical calculations, spectroscopic data, and device performance data. See DOI: https://doi.org/10.1039/d5sc04370k. CCDC 2463502 (**NTPCF**), 2463503 (**NTPH-B**) and 2463504 (**NTPH-O**) contain the supplementary crystallographic data for this paper.[79a–c]

Acknowledgements

The authors gratefully acknowledge the funding support from CSIR, DST, SERB, and DCPC, Government of India. Support from the SC-XRD Lab, SAIF, IIT Madras, for assistance with single-crystal X-ray diffraction data collection and structure refinement is also duly acknowledged. Financial support from the CSIR-FTT Project (MLP-0081), DST-AISRF (DST/INT/AUS/P-74/2017), the DST Nanomission Project (DST/NM/TUE/EE-02/2019-1), and the CSIR-NIIST DCPC Center of Excellence (PC-II-25014/3/2022-PC II-CPC, FTS: 3019123) is gratefully acknowledged. J. J. also acknowledges support from SERB under the CRG scheme (CRG/2022/005710).

Notes and references

1 P. Ganesan, R. Ranganathan, Y. Chi, X.-K. Liu, C.-S. Lee, S.-H. Liu, G.-H. Lee, T.-C. Lin, Y.-T. Chen and P.-T. Chou, Functional Pyrimidine-Based Thermally Activated Delay Fluorescence Emitters: Photophysics, Mechanochromism, and Fabrication of Organic Light-Emitting Diodes, *Chem. – Eur. J.*, 2017, **23**, 2858–2866.

2 X. Ban, F. Chen, Y. Liu, J. Pan, A. Zhu, W. Jiang and Y. Sun, Design of efficient thermally activated delayed fluorescence blue host for high performance solution-processed hybrid white organic light emitting diodes, *Chem. Sci.*, 2019, **10**, 3054–3064.

3 I. S. Park, K. Matsuo, N. Aizawa and T. Yasuda, High-Performance Dibenzoheteraborin-Based Thermally Activated Delayed Fluorescence Emitters: Molecular Architectonics for Concurrently Achieving Narrowband Emission and Efficient Triplet–Singlet Spin Conversion, *Adv. Funct. Mater.*, 2018, **28**, 1802031.

4 Z. Yang, Z. Mao, Z. Xie, Y. Zhang, S. Liu, J. Zhao, J. Xu, Z. Chi and M. P. Aldred, Recent advances in organic thermally activated delayed fluorescence materials, *Chem. Soc. Rev.*, 2017, **46**, 915–1016.

5 P. Rajamalli, N. Senthilkumar, P. Gandeepan, P.-Y. Huang, M.-J. Huang, C.-Z. Ren-Wu, C.-Y. Yang, M.-J. Chiu, L.-K. Chu, H.-W. Lin and C.-H. Cheng, A New Molecular Design Based on Thermally Activated Delayed Fluorescence for Highly Efficient Organic Light Emitting Diodes, *J. Am. Chem. Soc.*, 2016, **138**, 628–634.

6 Y.-X. Jin, H. Liu, Y. Zhao, Z.-Q. Chen, S. Hu, K. Zhang, M.-K. Fung, D.-Y. Zhou, L.-S. Liao and J. Fan, A simple molecular design strategy for efficient deep-red thermally activated delayed fluorescence emitter, *Chem. Eng. J.*, 2024, **488**, 150782.

7 C.-C. Lin, M.-J. Huang, M.-J. Chiu, M.-P. Huang, C.-C. Chang, C.-Y. Liao, K.-M. Chiang, Y.-J. Shiau, T.-Y. Chou, L.-K. Chu, H.-W. Lin and C.-H. Cheng, Molecular Design of Highly Efficient Thermally Activated Delayed Fluorescence Hosts for Blue Phosphorescent and Fluorescent Organic Light-Emitting Diodes, *Chem. Mater.*, 2017, **29**, 1527–1537.

8 D. Barman, R. Gogoi, K. Narang and P. K. Iyer, Recent Developments on Multi-Functional Metal-Free Mechanochromic Luminescence and Thermally Activated Delayed Fluorescence Organic Materials, *Front. Chem.*, 2020, **8**, 531643.

9 M. Banerjee and A. Anoop, Exploring the Theoretical Foundations of Thermally Activated Delayed Fluorescence (TADF) Emission: A Comprehensive TD-DFT Study on Phenothiazine Systems, *Chem. – Eur. J.*, 2024, **30**, e202304206.

10 C. Lee, Y.-T. Lee, C.-Y. Chan, C. W. Park, S. Lee, H. I. Kwon, D. Boo, Y. Tsuchiya, S. Y. Lee and C. Adachi, Regioisomer Effect of Pyrene on Multi-Resonance Emitters and Their Application for Hyperfluorescence Organic Light-Emitting Diodes, *Adv. Opt. Mater.*, 2025, **13**, 2402862.

11 H. Jiang, J. Jin and W.-Y. Wong, High-Performance Multi-Resonance Thermally Activated Delayed Fluorescence Emitters for Narrowband Organic Light-Emitting Diodes, *Adv. Funct. Mater.*, 2023, **33**, 2306880.

12 X.-K. Liu, Z. Chen, C.-J. Zheng, C.-L. Liu, C.-S. Lee, F. Li, X.-M. Ou and X.-H. Zhang, Prediction and Design of Efficient Exciplex Emitters for High-Efficiency, Thermally Activated Delayed-Fluorescence Organic Light-Emitting Diodes, *Adv. Mater.*, 2015, **27**, 2378–2383.

13 G. V. Mageswari, Y. Chitose, Y. Tsuchiya, J.-H. Lin and C. Adachi, Rational Molecular Design for Balanced Locally Excited and Charge- Transfer Nature for Two-Photon Absorption Phenomenon and Highly Efficient TADF-Based OLEDs, *Angew. Chem., Int. Ed.*, 2025, **64**, e202420417.

14 Z. Pang, S. Shen, X. Xie, X. Lv, Y. Liu, J. Liu and Y. Wang, Optimizing through-space charge transfer in thermally activated delayed fluorescence emitters for enhanced OLED efficiency, *J. Mater. Chem. C*, 2025, **13**, 9232–9238.

15 Y. Song, K. Zhang, Y. Li and L. He, Combining planar donor and acceptor in through-space charge-transfer emitters: Enhanced radiative decays, regioisomeric control and high-performance organic light-emitting diodes, *Chem. Eng. J.*, 2025, **521**, 166755.

16 S. K. Behera, S. Y. Park and J. Gierschner, Dual Emission: Classes, Mechanisms, and Conditions, *Angew. Chem., Int. Ed.*, 2021, **60**, 22624–22638.

17 H. Liu, G. Pan, Z. Yang, Y. Wen, X. Zhang, S.-T. Zhang, W. Li and B. Yang, Dual-Emission of Fluorescence and Room-Temperature Phosphorescence for Ratiometric and Colorimetric Oxygen Sensing and Detection Based on Dispersion of Pure Organic Thianthrene Dimer in Polymer Host, *Adv. Opt. Mater.*, 2022, **10**, 2102814.

18 J. Rui, J. Pu, Z. Chen, H. Tang, L. Wang, S.-J. Su and D. Cao, Single-molecule white organic light-emitting diodes based on dual-conformation diindolophenthiazine derivatives, *J. Mater. Chem. C*, 2024, **12**, 9182–9188.

19 D. Tu, P. Leong, S. Guo, H. Yan, C. Lu and Q. Zhao, Highly Emissive Organic Single-Molecule White Emitters by Engineering o-Carborane-Based Luminophores, *Angew. Chem., Int. Ed.*, 2017, **56**, 11370–11374.

20 Q.-Y. Yang and J.-M. Lehn, Bright White-Light Emission from a Single Organic Compound in the Solid State, *Angew. Chem., Int. Ed.*, 2014, **53**, 4572–4577.

21 C. Li, R. S. Nobuyasu, Y. Wang, F. B. Dias, Z. Ren, M. R. Bryce and S. Yan, Solution-Processable Thermally Activated Delayed Fluorescence White OLEDs Based on Dual-Emission Polymers with Tunable Emission Colors and Aggregation-Enhanced Emission Properties, *Adv. Opt. Mater.*, 2017, **5**, 1700435.

22 C. Si, T. Wang, Y. Xu, D. Lin, D. Sun and E. Zysman-Colman, A temperature sensor with a wide spectral range based on a dual-emissive TADF dendrimer system, *Nat. Commun.*, 2024, **15**, 7439.

23 M. Gužauskas, E. Narbutaitis, D. Volyniuk, G. V. Baryshnikov, B. F. Minaev, H. Ågren, Y.-C. Chao, C.-C. Chang, M. Rutkis and J. V. Grazulevicius, Polymorph acceptor-based triads with photoinduced TADF for UV sensing, *Chem. Eng. J.*, 2021, **425**, 131549.

24 M. Yang, I. S. Park, Y. Miyashita, K. Tanaka and T. Yasuda, Mechanochromic Delayed Fluorescence Switching in Propeller-Shaped Carbazole–Isophthalonitrile Luminogens with Stimuli-Responsive Intramolecular Charge-Transfer Excited States, *Angew. Chem., Int. Ed.*, 2020, **59**, 13955–13961.

25 L. Zhan, Z. Chen, S. Gong, Y. Xiang, F. Ni, X. Zeng, G. Xie and C. Yang, A Simple Organic Molecule Realizing Simultaneous TADF, RTP, AIE, and Mechanoluminescence: Understanding the Mechanism Behind the Multifunctional Emitter, *Angew. Chem., Int. Ed.*, 2019, **58**, 17651–17655.

26 X. Zeng, T. Zhou, J. Liu, K. Wu, S. Li, X. Xiao, Y. Zhang, S. Gong, G. Xie and C. Yang, Incorporating Thermally Activated Delayed Fluorescence into Mechanochromic Luminescent Emitters: High-Performance Solution-Processed Yellow Organic Light Emitting Diodes, *Adv. Opt. Mater.*, 2018, **6**, 1801071.

27 K. Zheng, H. Yang, F. Ni, Z. Chen, S. Gong, Z. Lu and C. Yang, Multifunctional Thermally Activated Delayed Fluorescence Emitters and Insight into Multicolor-Mechanochromism Promoted by Weak Intra- and Intermolecular Interactions, *Adv. Opt. Mater.*, 2019, **7**, 1900727.

28 A. Chatterjee, J. Chatterjee, S. Sappati, R. Tanwar, M. D. Ambhore, H. Arfin, R. M. Umesh, M. Lahiri, P. Mandal and P. Hazra, Engineering TADF, mechanochromism, and second harmonic up-conversion properties in regioisomeric substitution space, *Chem. Sci.*, 2023, **14**, 13832–13841.

29 R. Ishimatsu, S. Matsunami, K. Shizu, C. Adachi, K. Nakano and T. Imato, Solvent Effect on Thermally Activated Delayed Fluorescence by 1,2,3,5-Tetrakis(carbazol-9-yl)-4,6-dicyanobenzene, *J. Phys. Chem. A*, 2013, **117**, 5607–5612.

30 J. Jiang, C. Hu, J. Liu, L. Ma, Y. Wang and J. Guo, The dual-band emissions, multicolor continuous mechanochromisms, and application based on a single luminogen, *J. Alloys Compd.*, 2024, **1008**, 176594.

31 M. Okazaki, Y. Takeda, P. Data, P. Pander, H. Higginbotham, A. P. Monkman and S. Minakata, Thermally activated delayed fluorescent phenothiazine–dibenzo[a,j]phenazine–phenothiazine triads exhibiting tricolor-changing mechanochromic luminescence, *Chem. Sci.*, 2017, **8**, 2677–2686.

32 H. Wu, Y.-Z. Shi, K. Wang, J. Yu and X.-H. Zhang, Conformational isomeric thermally activated delayed fluorescence (TADF) emitters: mechanism, applications, and perspectives, *Phys. Chem. Chem. Phys.*, 2023, **25**, 2729–2741.

33 P. Xue, J. Ding, P. Chen, P. Wang, B. Yao, J. Sun, J. Sun and R. Lu, Mechanical force-induced luminescence enhancement and chromism of a nonplanar D–A phenothiazine derivative, *J. Mater. Chem. C*, 2016, **4**, 5275–5280.

34 P. Khammultri, W. Kitisriworaphan, P. Chasing, S. Namuangruk, T. Sudyoadsuk and V. Promarak, Efficient white light-emitting polymers from dual thermally activated delayed fluorescence chromophores for non-doped solution processed white electroluminescent devices, *Polym. Chem.*, 2021, **12**, 1030–1039.

35 C. Li, Y. Xu, Y. Liu, Z. Ren, Y. Ma and S. Yan, Highly efficient white-emitting thermally activated delayed fluorescence polymers: Synthesis, non-doped white OLEDs and electroluminescent mechanism, *Nano Energy*, 2019, **65**, 104057.

36 H. Tanaka, K. Shizu, H. Nakanotani and C. Adachi, Dual Intramolecular Charge-Transfer Fluorescence Derived from a Phenothiazine-Triphenyltriazine Derivative, *J. Phys. Chem. C*, 2014, **118**, 15985–15994.

37 M. Kumar and P. Kumar, in *White Light Emitting Materials: Illuminating Brilliance*, ed. M. Kumar and P. Kumar, Springer Nature Singapore, Singapore, 2024, pp. 23–55.

38 B. Xu, Y. Mu, Z. Mao, Z. Xie, H. Wu, Y. Zhang, C. Jin, Z. Chi, S. Liu, J. Xu, Y.-C. Wu, P.-Y. Lu, A. Lien and M. R. Bryce, Achieving remarkable mechanochromism and white-light emission with thermally activated delayed fluorescence through the molecular heredity principle, *Chem. Sci.*, 2016, **7**, 2201–2206.

39 L. Lian, S. Wang, H. Ding, G. Liang, Y.-B. Zhao, H. Song, X. Lan, J. Gao, R. Chen, D. Zhang and J. Zhang, Single-Component White-Light Emitters with Excellent Color Rendering Indexes and High Photoluminescence Quantum Efficiencies, *Adv. Opt. Mater.*, 2022, **10**, 2101640.

40 Z. Chen, C.-L. Ho, L. Wang and W.-Y. Wong, Single-Molecular White-Light Emitters and Their Potential WOLED Applications, *Adv. Mater.*, 2020, **32**, 1903269.

41 S. K. Behera, R. Kainda, S. Basu and Y. S. Chaudhary, Single organic molecular systems for white light emission and their classification with associated emission mechanism, *Appl. Mater. Today*, 2022, **27**, 101407.

42 Z. Xie, C. Chen, S. Xu, J. Li, Y. Zhang, S. Liu, J. Xu and Z. Chi, White-light emission strategy of a single organic compound with aggregation-induced emission and delayed fluorescence properties, *Angew. Chem., Int. Ed.*, 2015, **54**, 7181–7184.

43 K. Wang, Y.-Z. Shi, C.-J. Zheng, W. Liu, K. Liang, X. Li, M. Zhang, H. Lin, S.-L. Tao, C.-S. Lee, X.-M. Ou and X.-H. Zhang, Control of Dual Conformations: Developing Thermally Activated Delayed Fluorescence Emitters for Highly Efficient Single-Emitter White Organic Light-Emitting Diodes, *ACS Appl. Mater. Interfaces*, 2018, **10**, 31515–31525.

44 B. Li, Z. Li, F. Guo, J. Song, X. Jiang, Y. Wang, S. Gao, J. Wang, X. Pang, L. Zhao and Y. Zhang, Realizing Efficient Single Organic Molecular White Light-Emitting Diodes from Conformational Isomerization of Quinazoline-Based Emitters, *ACS Appl. Mater. Interfaces*, 2020, **12**, 14233–14243.

45 F. Khan and R. Misra, Recent advances in the development of phenothiazine and its fluorescent derivatives for optoelectronic applications, *J. Mater. Chem. C*, 2023, **11**, 2786–2825.

46 M. Gao, R. Wu, Y. Zhang, Y. Meng, M. Fang, J. Yang and Z. Li, New Molecular Photoswitch Based on the Conformational Transition of Phenothiazine Derivatives and Corresponding Triplet Emission Properties, *J. Am. Chem. Soc.*, 2025, **147**, 2653–2663.

47 J. Daub, R. Engl, J. Kurzawa, S. E. Miller, S. Schneider, A. Stockmann and M. R. Wasielewski, Competition between Conformational Relaxation and Intramolecular Electron Transfer within Phenothiazine—Pyrene Dyads, *J. Phys. Chem. A*, 2001, **105**, 5655–5665.

48 J. Zhang, M. Zhu, Y. Lu, X. Zhang, S. Xiao, H. Lan and T. Yi, Design of Stimuli-Responsive Phenothiazine Derivatives with Triplet-Related Dual Emission and High-Contrast Mechanochromism Guided by Polymorph Prediction, *Chem. – Eur. J.*, 2022, **28**, e202200458.

49 T. Song, H. Liu, J. Ren and Z. Wang, Achieving TADF and RTP with Stimulus-Responsiveness and Tunability from Phenothiazine-Based Donor—Acceptor Molecules, *Adv. Opt. Mater.*, 2024, **12**, 2301215.

50 Y. Gong, M. Xia, X. Wang, Y. Wang, Y. Jia, Y. Tao, J. Zhang, J. Yang, M. Fang, Q.-H. Yang, Z. Li and B. Z. Tang, Exploring the role of phenothiazine conformations and their interconversion on the electrochemical behaviour of organic electrodes, *J. Mater. Chem. A*, 2025, **13**, 20496–20503.

51 K. Stavrou, L. G. Franca, T. Böhmer, L. M. Duben, C. M. Marian and A. P. Monkman, Unexpected Quasi-Axial Conformer in Thermally Activated Delayed Fluorescence

DMAC-TRZ, Pushing Green OLEDs to Blue, *Adv. Funct. Mater.*, 2023, **33**, 2300910.

52 Y. Gao, W. Yuan, Y. Li, A. Huang, Y. Fang, A. Li, K. Wang, B. Zou, Q. Li and Z. Li, Accurately adjusted phenothiazine conformations: reversible conformation transformation at room temperature and self-recoverable stimuli-responsive phosphorescence, *Light: Sci. Appl.*, 2025, **14**, 99.

53 C. Li, J. Liang, B. Liang, Z. Li, Z. Cheng, G. Yang and Y. Wang, An Organic Emitter Displaying Dual Emissions and Efficient Delayed Fluorescence White OLEDs, *Adv. Opt. Mater.*, 2019, **7**, 1801667.

54 B. Zhang, S. Liu, J. Pei, Z. Wang, Y. Chen, Q. Jia, C. Hao, X. Lei, Z. Wu, Z. Yang, G. Zhou and D. Wang, Multiple stimuli-responsive dual-emission material with locked diverse conformations for multimodal anti-counterfeiting and single-molecule white electroluminescence, *Chem. Eng. J.*, 2025, **513**, 162788.

55 X. Long, Z. Ma, H. Dai, Y. Wang, H. Xie, X. Ge, Z. Yang, J. Zhao, W. Hong and Z. Chi, Achieving Multi-Color Emissive Organic Light-Emitting Diodes With Single-Component Molecule Through Conformational Regulation, *Aggregate*, 2025, **6**, e70006.

56 J. Yang, J. Qin, P. Geng, J. Wang, M. Fang and Z. Li, Molecular Conformation-Dependent Mechanoluminescence: Same Mechanical Stimulus but Different Emissive Color over Time, *Angew. Chem., Int. Ed.*, 2018, **57**, 14174–14178.

57 B. Kumari, R. Dahiwadkar and S. Kanvah, White light emission from AIE-active luminescent organic materials, *Aggregate*, 2022, **3**, e191.

58 N. A. Kukhta and M. R. Bryce, Dual emission in purely organic materials for optoelectronic applications, *Mater. Horiz.*, 2021, **8**, 33–55.

59 A. Ekbote, S. M. Mobin and R. Misra, Stimuli-responsive phenothiazine-based donor–acceptor isomers: AIE, mechanochromism and polymorphism, *J. Mater. Chem. C*, 2020, **8**, 3589–3602.

60 P. Data, M. Okazaki, S. Minakata and Y. Takeda, Thermally activated delayed fluorescence vs. room temperature phosphorescence by conformation control of organic single molecules, *J. Mater. Chem. C*, 2019, **7**, 6616–6621.

61 W. Liu, Z. Chen, C.-J. Zheng, X.-K. Liu, K. Wang, F. Li, Y.-P. Dong, X.-M. Ou and X.-H. Zhang, A novel nicotinonitrile derivative as an excellent multifunctional blue fluorophore for highly efficient hybrid white organic light-emitting devices, *J. Mater. Chem. C*, 2015, **3**, 8817–8823.

62 M. Gao, Y. Tian, X. Li, Y. Gong, M. Fang, J. Yang and Z. Li, The Effect of Molecular Conformations and Simulated "Self-Doping" in Phenothiazine Derivatives on Room-Temperature Phosphorescence, *Angew. Chem., Int. Ed.*, 2023, **62**, e202214908.

63 M. Szymańska and I. Majerz, Geometry and electron density of phenothazines, *J. Mol. Struct.*, 2020, **1200**, 127095.

64 D.-G. Chen, Y. Chen, C.-H. Wu, Y.-A. Chen, M.-C. Chen, J.-A. Lin, C.-Y. Huang, J. Su, H. Tian and P.-T. Chou, A New Scope of Phenothiazines: The Steric Strain Induced Planarization and Excimer Formation, *Angew. Chem.*, 2019, **58**, 13297–13301.

65 A. Klimash, P. Pander, W. T. Klooster, S. J. Coles, P. Data, F. B. Dias and P. J. Skabara, Intermolecular interactions in molecular crystals and their effect on thermally activated delayed fluorescence of helicene-based emitters, *J. Mater. Chem. C*, 2018, **6**, 10557–10568.

66 Y. Yang, A. Li, Z. Ma, J. Liu, W. Xu, Z. Ma and X. Jia, Dibenzo [a,c]phenazine-phenothiazine dyad: AIEE, polymorphism, distinctive mechanochromism, high sensitivity to pressure, *Dyes Pigm.*, 2020, **181**, 108575.

67 A. D. Becke, Density-functional thermochemistry. I. The effect of the exchange-only gradient correction, *J. Chem. Phys.*, 1992, **96**, 2155–2160.

68 F. Weigend and R. Ahlrichs, Balanced basis sets of split valence, triple zeta valence and quadruple zeta valence quality for H to Rn: Design and assessment of accuracy, *Phys. Chem. Chem. Phys.*, 2005, **7**, 3297–3305.

69 M. Moral, L. Muccioli, W. J. Son, Y. Olivier and J. C. Sancho-García, Theoretical Rationalization of the Singlet–Triplet Gap in OLEDs Materials: Impact of Charge-Transfer Character, *J. Chem. Theory Comput.*, 2015, **11**, 168–177.

70 G. Ricci, J.-C. Sancho-García and Y. Olivier, Establishing design strategies for emissive materials with an inverted singlet–triplet energy gap (INVEST): a computational perspective on how symmetry rules the interplay between triplet harvesting and light emission, *J. Mater. Chem. C*, 2022, **10**, 12680–12698.

71 M. Bursch, J.-M. Mewes, A. Hansen and S. Grimme, Best-Practice DFT Protocols for Basic Molecular Computational Chemistry, *Angew. Chem., Int. Ed.*, 2022, **61**, e202205735.

72 S. Grimme, S. Ehrlich and L. Goerigk, Effect of the damping function in dispersion corrected density functional theory, *J. Comput. Chem.*, 2011, **32**, 1456–1465.

73 R. Izsák and F. Neese, Speeding up spin-component-scaled third-order pertubation theory with the chain of spheres approximation: the COSX-SCS-MP3 method, *Mol. Phys.*, 2013, **111**, 1190–1195.

74 F. Neese, The ORCA program system, *Wiley Interdiscip. Rev.:Comput. Mol. Sci.*, 2012, **2**, 73–78.

75 M. K. Etherington, F. Franchello, J. Gibson, T. Northey, J. Santos, J. S. Ward, H. F. Higginbotham, P. Data, A. Kurowska, P. L. Dos Santos, D. R. Graves, A. S. Batsanov, F. B. Dias, M. R. Bryce, T. J. Penfold and A. P. Monkman, Regio- and conformational isomerization critical to design of efficient thermally-activated delayed fluorescence emitters, *Nat. Commun.*, 2017, **8**, 14987.

76 Z. He, X. Cai, Z. Wang, D. Chen, Y. Li, H. Zhao, K. Liu, Y. Cao and S.-J. Su, Reversible switching between normal and thermally activated delayed fluorescence towards "smart" and single compound white-light luminescence via controllable conformational distribution, *Sci. China Chem.*, 2018, **61**, 677–686.

77 P. Borowicz, J. Herbich, A. Kapturkiewicz, R. Anulewicz-Ostrowska, J. Nowacki and G. Grampp, Nature of the lowest triplet states of 4'-substituted N-

phenylphenothiazine derivatives, *Phys. Chem. Chem. Phys.*, 2000, **2**, 4275–4280.

78 S. J. N. Dixit and N. Agarwal, Blue shifted phosphorescence (3LE) as compared to charge transfer singlet emission (1CT) in fluorenone-amine dyads under ambient conditions, *J. Mol. Struct.*, 2024, **1316**, 139028.

79 (*a*) CCDC 2463502: Experimental Crystal Structure Determination, 2025, DOI: **10.5517/ccdc.csd.cc2npgtn**; (*b*) CCDC 2463503: Experimental Crystal Structure Determination, 2025, DOI: **10.5517/ccdc.csd.cc2npgvp**; (*c*) CCDC 2463504: Experimental Crystal Structure Determination, 2025, DOI: **10.5517/ccdc.csd.cc2npgwq**.